

Vector solitons in parity-time-symmetric mixed linear-nonlinear lattices with fractional diffraction

Xing Zhu(朱兴), Milivoj R. Belić, Dumitru Mihalache, Qinfang Xu(许勤芳), and Liangwei Zeng(曾亮维)
Citation: Chin. Phys. B, 2026, 35 (**8**): 080505. DOI: 10.1088/1674-1056/ae1455
http://cpb.iphy.ac.cn; http://iopscience.iop.org/cpb

What follows is a list of articles you may be interested in

Hybrid computational analysis of fractional optical soliton structures in a dispersive Schrödinger model with applications in nonlinear optics

Mati ur Rahman, Sonia Akram, and Laila A. AL-Essa
Chin. Phys. B, 2026, 35 (**7**): 070503. DOI: 10.1088/1674-1056/ae5808

A novel (2+1)-dimensional complex coupled dispersionless system: Darboux transformation and multisolitons

H. W. A. Riaz and Ji Lin(林机)
Chin. Phys. B, 2025, 34 (**9**): 090502. DOI: 10.1088/1674-1056/adceff

High-order effect on the transmission of two optical solitons

Houhui Yi(伊厚会), Yanli Yao(姚延立), Xin Zhang(张鑫), and Guoli Ma(马国利)
Chin. Phys. B, 2023, 32 (**10**): 100509. DOI: 10.1088/1674-1056/aceeec

Soliton fusion and fission for the high-order coupled nonlinear Schrödinger system in fiber lasers

Tian-Yi Wang(王天一), Qin Zhou(周勤), and Wen-Jun Liu(刘文军)
Chin. Phys. B, 2022, 31 (**2**): 020501. DOI: 10.1088/1674-1056/ac2d22

Solitons in nonlinear systems and eigen-states in quantum wells

Li-Chen Zhao(赵立臣), Zhan-Ying Yang(杨战营), Wen-Li Yang(杨文力)
Chin. Phys. B, 2019, 28 (**1**): 010501. DOI: 10.1088/1674-1056/28/1/010501

Vector solitons in parity–time-symmetric mixed linear–nonlinear lattices with fractional diffraction

Xing Zhu(朱兴)[1], Milivoj R. Belić[2], Dumitru Mihalache[3], Qinfang Xu(许勤芳)[1], and Liangwei Zeng(曾亮维)[1,4,†]

[1] *School of Arts and Sciences, Guangzhou Maritime University, Guangzhou* 510725, *China*
[2] *College of Science and Engineering, Hamad Bin Khalifa University,* 23874 *Doha, Qatar*
[3] *Horia Hulubei National Institute of Physics and Nuclear Engineering,* 077125 *Magurele, Bucharest, Romania*
[4] *College of Physics and Optoelectronic Engineering, Shenzhen University, Shenzhen* 518060, *China*

(Received 10 September 2025; revised manuscript received 14 October 2025; accepted manuscript online 17 October 2025)

We demonstrate that $\mathcal{PT}$-symmetric mixed linear-nonlinear lattices can sustain mixed-gap vector solitons in the coupled nonlinear Schrödinger equations with fractional diffraction. Here, mixed-gap vector solitons refer to solitons whose first and second components exist in different band gaps. In this work, the first component is a fundamental soliton, while the second is a dipole. When the propagation constant of the first component is fixed, the soliton power of the first component decreases as the propagation constant of the second component increases. Conversely, the power of the second component increases with its own propagation constant. We study cases with both large and small values of the Lévy index. We also study the stability of these solitons, using linear stability analysis and perturbed propagations. Interestingly, the stability domains of vector solitons with a large Lévy index are consistently much wider than those with a small Lévy index.

Keywords: parity–time-symmetry, vector solitons, linear–nonlinear lattices, fractional diffraction, nonlinear optics

PACS: 05.45.Yv, 42.65.Tg, 42.81.Dp

DOI: 10.1088/1674-1056/ae1455 **CSTR:** 32038.14.CPB.ae1455

1. Introduction

The formation of solitons[1–5] is an interesting topic in nonlinear physics, which has attracted a great deal of attention in the past few decades, especially in the fields of nonlinear optics[6–12] and Bose–Einstein condensates.[13–19] Generally, solitons are generated by the balance of dispersion/diffraction and nonlinear effects. With the help of linear and nonlinear potentials, many types of solitons have been reported,[2,20] including fundamental solitons,[21,22] dipole solitons,[23] multipole solitons,[24] vortex solitons,[25] and coupled solitons.[26,27] Especially interesting settings are the periodic linear and nonlinear potentials, among which the former are called the linear lattices[28] and the latter the nonlinear lattices.[29,30]

The parity–time ($\mathcal{PT}$) symmetry[31,32] of physical systems has produced much interest at the turn of the century.[33–36] It represents a great extension of physical settings from Hermitian to non-Hermitian quantum mechanics.[3,37,38] It also turned out to be highly relevant for other fields of physics, such as photonics, where systems that do not obey Hermiticity are quite common. For example, materials with distributed loss and gain, or lasing media in lossy resonators, are typical systems that lead to non-Hermitian behavior.[33] With $\mathcal{PT}$ symmetry, non-Hermitian Hamiltonians may exhibit completely real spectra, provided only the system obeys the symmetry. Thus, Hamiltonians with a $\mathcal{PT}$-symmetric lattice V can have real spectra if the condition $V(x) = V^*(-x)$ is satisfied.[33–36] With fascinating $\mathcal{PT}$-symmetric lattices, many types of solitons have been investigated both theoretically[39–48] and experimentally.[49]

Fractional quantum mechanics is another important extension of quantum mechanics, also achieved at the turn of the century.[50–52] By replacing the Brownian paths in the Feynman integral with Lévy-like paths, the nonlinear Schrödinger equation (NLSE) turns into the nonlinear fractional Schrödinger equation (NLFSE). After experimental realizations of the fractional derivative were proposed,[53,54] solitons in NLFSE have gained considerable attention, and many types of solitons have been investigated,[55,56] including fundamental solitons,[57–59] dipole solitons,[60,61] multipole solitons,[62] accessible solitons,[63] vortex solitons,[64,65] surface solitons,[66] and coupled solitons,[67] to name a few. Despite the fact that so many types of solitons have been reported, vector solitons[68–71] in the NLFSE warrant additional attention, especially in physical settings with $\mathcal{PT}$ symmetry.

In this work, we study mixed-gap vector solitons in parity–time-symmetric mixed linear–nonlinear lattices with fractional diffraction. Note also that we focus on mixed vector solitons, where the first component of the coupled soliton exists in the semi-infinite band gap, while the second component exists in the first finite band gap. The cases with both

†Corresponding author. E-mail: liangweizeng@gzmtu.edu.cn

© 2026 Chinese Physical Society and IOP Publishing Ltd. All rights, including for text and data mining, AI training, and similar technologies, are reserved.

small and large values of the Lévy index are included. We are not aware of any work in the literature that investigated such systems.

The rest of this paper is arranged as follows. The theoretical model and the method of linear stability analysis are introduced in Section 2. The numerical results are displayed in Section 3, which is divided into three subsections. The numerical results with large and small Lévy indices are presented in Subsection 3.1 and Subsection 3.2, while the varied nonlinear lattice is considered in Subsection 3.3. Finally, we conclude this work in Section 4.

2. Model and its linear stability analysis

The coupled one-dimensional NLFSEs with parity–time-symmetric mixed linear–nonlinear lattices are employed to describe the propagation of vector solitons in our model. They can be written in the following dimensionless form:

$$\begin{aligned} \mathrm{i}\frac{\partial U_1}{\partial z} &= \left(-\frac{\partial^2}{\partial x^2}\right)^{\alpha/2} U_1 - V_1 U_1 - V_2\left(|U_1|^2+|U_2|^2\right)U_1, \\ \mathrm{i}\frac{\partial U_2}{\partial z} &= \left(-\frac{\partial^2}{\partial x^2}\right)^{\alpha/2} U_2 - V_1 U_2 - V_2\left(|U_1|^2+|U_2|^2\right)U_2. \end{aligned} \quad (1)$$

Here, $U_{1,2}$ and z are the field amplitudes and the propagation distance, respectively. α denotes the Lévy index, whose range of values is $1<\alpha\leq 2$. V_1 and V_2 represent the parity–time-symmetric linear and nonlinear lattices. In this work, the fractional diffraction is defined as

$$\left(-\frac{\partial^2}{\partial x^2}\right)^{\alpha/2} U(x) = \frac{1}{2\pi}\int_{-\infty}^{+\infty} \mathrm{d}t|t|^{\alpha}\int_{-\infty}^{+\infty}\mathrm{d}\xi\,\mathrm{e}^{\mathrm{i}t(x-\xi)}U(\xi). \quad (2)$$

The expression of linear lattices can take many forms. We opt for

$$V_1 = V_{10}\,[\sin^2(x)+\mathrm{i}W_{10}\,\sin(2x)], \quad (3)$$

where V_{10} and W_{10} are constant real parameters. The form of nonlinear lattices is chosen as

$$V_2 = 1+V_{20}\,\cos^2(x)+\mathrm{i}W_{20}\,\sin(2x), \quad (4)$$

where V_{20} and W_{20} are also constant real parameters. With so many free parameters at our disposal, some restrictions must be imposed to keep focus on interesting novel phenomena. Without loss of generality, we fix the values of $V_{10}=5$ and $V_{20}=1$ throughout but vary the imaginary part W_{10} of the linear potential. Additionally, the imaginary part W_{20} of the nonlinear potential is kept constant at $W_{20}=0.5$, except in the last part of the paper, when it is changed to ascertain the corresponding changes in vector solitons. As is typical of $\mathcal{PT}$-symmetric systems, increasing imaginary parts from 0 eventually leads to a threshold value, at which the properties of solutions change dramatically.

Substituting $U_{1,2}=q_{1,2}\exp(\mathrm{i}\mu_{1,2}z)$ (where $\mu_{1,2}$ are the real propagation constants of the two components) into Eq. (1), one obtains equations for the stationary solutions of the form

$$\begin{aligned} -\mu_1 q_1 &= \left(-\frac{\partial^2}{\partial x^2}\right)^{\alpha/2} q_1 - V_1 q_1 - V_2\left(|q_1|^2+|q_2|^2\right)q_1, \\ -\mu_2 q_2 &= \left(-\frac{\partial^2}{\partial x^2}\right)^{\alpha/2} q_2 - V_1 q_2 - V_2\left(|q_1|^2+|q_2|^2\right)q_2. \end{aligned} \quad (5)$$

These equations are numerically solved by a method developed from the modified squared-operator iteration method.[72] In this article, we investigate vector solitons with $\mu_1\neq\mu_2$. The total power of a vector soliton is defined as $P=\int_{-\infty}^{+\infty}(|q_1|^2+|q_2|^2)\,\mathrm{d}x$, while the two partial powers are $P_1=\int_{-\infty}^{+\infty}|q_1|^2\,\mathrm{d}x$ and $P_2=\int_{-\infty}^{+\infty}|q_2|^2\,\mathrm{d}x$.

To consider gap solitons, one needs a band structure. To obtain a band structure of a lattice, one neglects nonlinearity and considers the linear equation

$$-\left(-\frac{\partial^2}{\partial x^2}\right)^{\alpha/2} q + V_1 q = \mu q. \quad (6)$$

The Bloch theorem tells us that the eigenfunctions of Eq. (6) can be written as $q=F_k(x)\exp(\mathrm{i}kx)$, where $F_k(x)$ is a periodic function, $F_k(x)=F_k(x+D)$. The period D ($D=\pi$ in this work) is also the period of the $\mathcal{PT}$-symmetric optical lattice and k ($-\pi/D\leq k\leq\pi/D$) is the Bloch wave number. To obtain Bloch bands, $F_k(x)$ and V_1 are expanded into series of plane waves: $F_k(x)=\sum_n A_n\exp(\mathrm{i}K_n x)$ and $V_1=\sum_m B_m\exp(\mathrm{i}K_m x)$, where $K_n=2\pi n/D$ and $B_m=\int_0^D V_1\exp(-\mathrm{i}K_m x)\,\mathrm{d}x/D$. By inserting these series into Eq. (6), one finally obtains the following eigenvalue equation:

$$-|k+K_n|^{\alpha}A_n+\sum_m B_m A_{n-m}=\mu A_n. \quad (7)$$

Equation (7) is an eigenvalue problem written in a matrix form. Here, it is solved numerically, and thus the band structure of $\mathcal{PT}$-symmetric optical lattices is obtained.

To determine the stability of vector solitons, we perform linear stability analysis. The perturbations $g_{1,2}(x)$ and $t_{1,2}(x)$ are added to the stationary solutions $q_{1,2}(x)$:

$$U_{1,2}(x,z)=[q_{1,2}(x)+g_{1,2}\mathrm{e}^{\delta z}+t_{1,2}^{*}\mathrm{e}^{\delta^{*}z}]\,\mathrm{e}^{\mathrm{i}\mu_{1,2}z}, \quad (8)$$

where δ is the growth rate and $|g_{1,2}|$, $|t_{1,2}|\ll|q_{1,2}|$. The superscript * denotes the complex conjugation. By substituting Eq. (8) into Eq. (1) and linearizing, one obtains the following coupled eigenvalue equations:

$$-\mathrm{i}\delta g_1=\hat{L}_1 g_1+V_2[(2|q_1|^2+|q_2|^2)g_1+q_1^2 t_1+q_1 q_2^{*}g_2+q_1 q_2 t_2],$$

$$
\begin{aligned}
-\mathrm{i}\delta t_1 &= -\hat{L}_1^* t_1 - V_2[(q_1^2)^* g_1 + (2|q_1|^2 + |q_2|^2)t_1 + q_1^* q_2^* g_2 + q_1^* q_2 t_2],\\
-\mathrm{i}\delta g_2 &= \hat{L}_2 g_2 + V_2[q_1^* q_2 g_1 + q_1 q_2 t_1 + (|q_1|^2 + 2|q_2|^2)g_2 + q_2^2 t_2],\\
-\mathrm{i}\delta t_2 &= -\hat{L}_2^* t_1 - V_2[q_1^* q_2^* g_1 + q_1 q_2^* t_1 + (q_2^2)^* g_2 + (|q_1|^2 + 2|q_2|^2)t_2],
\end{aligned} \tag{9}
$$

with $\hat{L}_1 = -(-\partial^2/\partial x^2)^{\alpha/2} + V_1 - \mu_1$ and $\hat{L}_2 = -(-\partial^2/\partial x^2)^{\alpha/2} + V_1 - \mu_2$. Equations (9) are numerically solved by the Fourier collocation method.[73] They provide eigenfunctions q_1 and q_2, and the spectrum of eigenvalues δ, which determines their stability. The vector solitons are linearly unstable if one or more real parts of eigenvalues δ are positive; otherwise, they are stable.

3. Numerical results

In this section, we focus on our numerical results, which include the profiles of vector solitons and their powers as functions of α, μ_1, and μ_2. Also included are linear stability analyses and propagations of both stable and unstable solitons. The section is divided into three subsections: the first two present solitons with large and small Lévy indices. Given that the Lévy index is restricted to the interval (1, 2], the representative value for a large index is chosen as $\alpha = 1.8$, while the representative value for a small index is $\alpha = 1.3$. Each of these subsections first displays the powers and profiles of both fundamental and dipole vector solitons, followed by a discussion of their stability. This analysis is performed for two representative values of the propagation constant μ_1. The third subsection deals with vector solitons when the nonlinear lattice is changed, by changing its imaginary part.

All results are obtained using the band structures depicted in Fig. 1. In fact, it is the same underlying band structure, presented for two values of α (large and small), and two values of W_{10} (sub-critical and critical). It should be recalled that an exciting feature of $\mathcal{PT}$ symmetry is its phase transition at a critical point, where spontaneous symmetry-breaking occurs and the eigenvalue spectrum becomes complex. This, naturally, induces instability in the obtained eigensolutions. The abrupt nature of this phase transition causes various exotic phenomena,[33] which are directly evident in the coalescence of eigenvectors and eigenvalues, visible as band merging in Figs. 1(c) and 1(d).

It should also be noted that, owing to the presence of two complex potentials in our model, instability can emerge even below the critical value of W_{10}, depending on the value of W_{20}. By varying W_{20}, while keeping W_{10} fixed, similar behavior is observed: there exists a critical value of W_{20} as well, at which instability is promoted. Curiously, instability may also appear when other parameters are varied, most notably propagation constants. Here, these behaviors are followed as functions of the propagation constants. To limit the computational load, we vary μ_2, while restricting μ_1 to a few fixed values.

For $W_{10} = 0.2$, the band structures for $\alpha = 1.8$ and $\alpha = 1.3$ are shown in Figs. 1(a) and (b). The semi-infinite gaps are $\mu \geq 3.1514$ and $\mu \geq 3.3435$, while the first finite gaps are $0.6045 \leq \mu \leq 2.8212$ and $0.9075 \leq \mu \leq 2.9401$, respectively. We further find that the Lévy index does not alter the critical threshold of W_{10}, at which the eigenvalues μ become complex. For different values of α, the phase transition point remains unchanged at $W_{10}^{\mathrm{th}} = 0.5$. The band structures at $W_{10} = 0.5$ are shown in Figs. 1(c) and 1(d). Further down (in the last subsection) we establish that the threshold value of the nonlinear lattice is $W_{20}^{\mathrm{th}} = 0.89$.

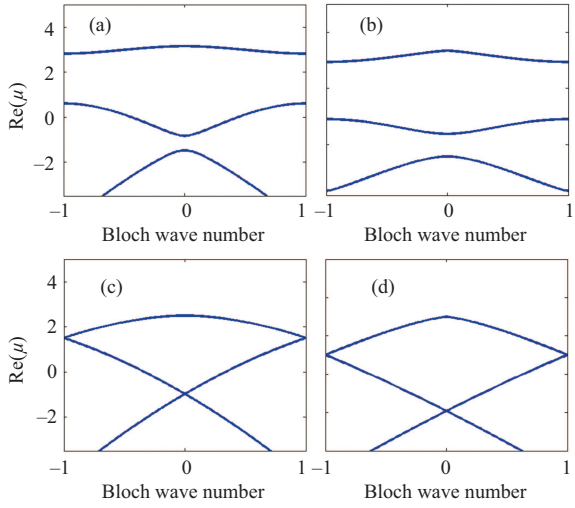


Fig. 1. (a)–(b) The band structures for $\alpha = 1.8$ and $\alpha = 1.3$, when $W_{10} = 0.2$. (c)–(d) The corresponding band structures for $W_{10} = 0.5$.

3.1. Vector solitons with a large Lévy index

Now, we consider soliton powers and profiles for a large Lévy index ($\alpha = 1.8$). First, we select $W_{10} = 0.2$, $W_{20} = 0.5$, $\mu_1 = 4.5$ (in the semi-infinite gap), and vary μ_2. Mixed-gap vector solitons are readily found under these conditions. Figures 2(a) and 2(b) portray partial powers and the total power of these solitons as functions of μ_2. It should be emphasized that the first component is a fundamental mode, while the second component is an out-of-phase dipole mode. The propagation constants of the first and second components belong to the semi-infinite and first finite gaps, respectively. The existence and stability domains are $0.96 \leq \mu_2 \leq 2.63$ and $0.96 \leq \mu_2 \leq 1.63$, respectively. Note also that this soliton family cannot reach the lower edge of the first Bloch band. The solitons are stable in a low-power region and unstable in a high-power region, as can be seen in panel (b), where the solid and dashed lines stand for the stable and unstable solitons, respectively.

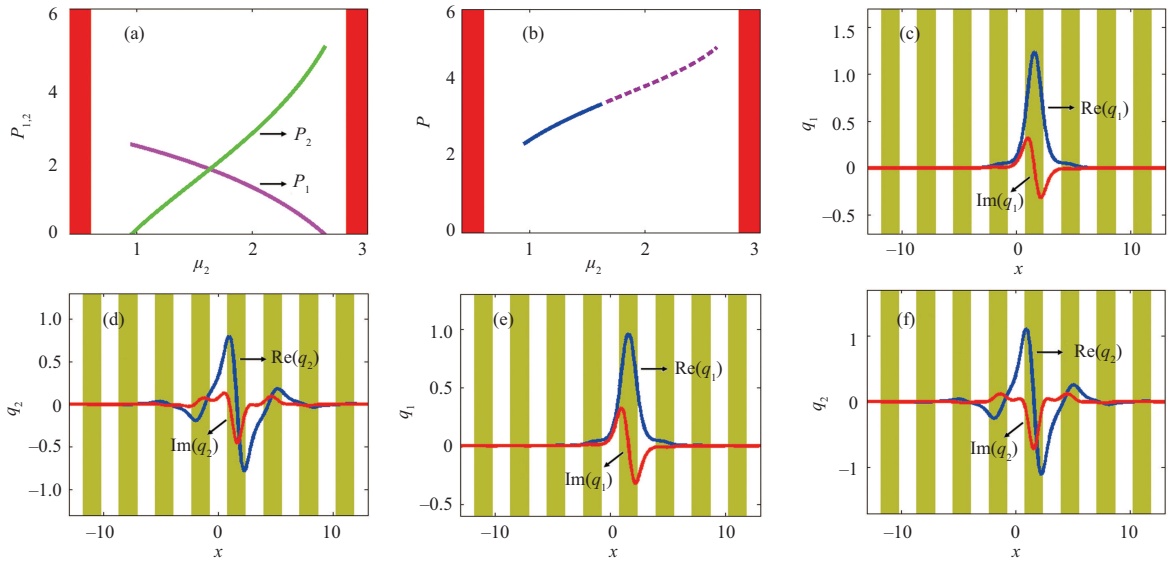


Fig. 2. (a) Partial powers of the two components of vector solitons (shaded red regions are Bloch bands) *versus* the propagation constant μ_2. (b) Total power of vector solitons (solid and dashed lines represent stable and unstable solitons) *versus* μ_2. (c)–(d) The profiles of the first and second components of the vector soliton for $\mu_2 = 1.5$. (e)–(f) The profiles of the first and second components for $\mu_2 = 2$. In all panels $\alpha = 1.8$, $W_{10} = 0.2$, $W_{20} = 0.5$, and $\mu_1 = 4.5$.

We present the profiles of the first and second components for the vector soliton at $\mu_2 = 1.5$ (in the first finite gap) in Figs. 2(c) and 2(d). The profiles for $\mu_2 = 2$ (also in the first finite gap) are shown in Figs. 2(e) and 2(f). A comparison of the profiles in panels (c)–(f) reveals that the width of both components remains nearly constant as μ_2 changes. In addition, the amplitude of the first component (q_1) decreases with μ_2, while the amplitude of the second component (q_2) increases. This behavior can also be inferred from the variation of soliton powers P_1 and P_2 with μ_2, in Fig. 2(a).

Next, we present linear-stability spectra and perturbed propagations for typical vector solitons from Fig. 2. Specifically, the spectrum and propagations of the soliton at $\mu_2 = 1.5$ in Figs. 2(c) and 2(d) are shown in Figs. 3(a)–3(c). Note that the left column in Fig. 3 displays the spectrum [given by Eqs. (9)], the middle column reports the propagation of the first component (U_1), and the right column depicts the propagation of the second component (U_2). According to Fig. 3(a), the mixed-gap soliton at $\mu_2 = 1.5$ is stable, as all real parts of δ are zero. The corresponding propagations in Figs. 3(b) and 3(c) are consistent with this result. In contrast, the spectrum and propagations of an unstable soliton at $\mu_2 = 2$ are presented in Figs. 3(d)–3(f) [with the corresponding profiles in Figs. 2(e)–2(f)]. As seen in Fig. 3(d), the real parts of two eigenvalues δ are greater than zero, indicating instability. Thus, such solitons are unstable, which is confirmed by their propagations in Figs. 3(e)–3(f), where both components suffer significant distortions.

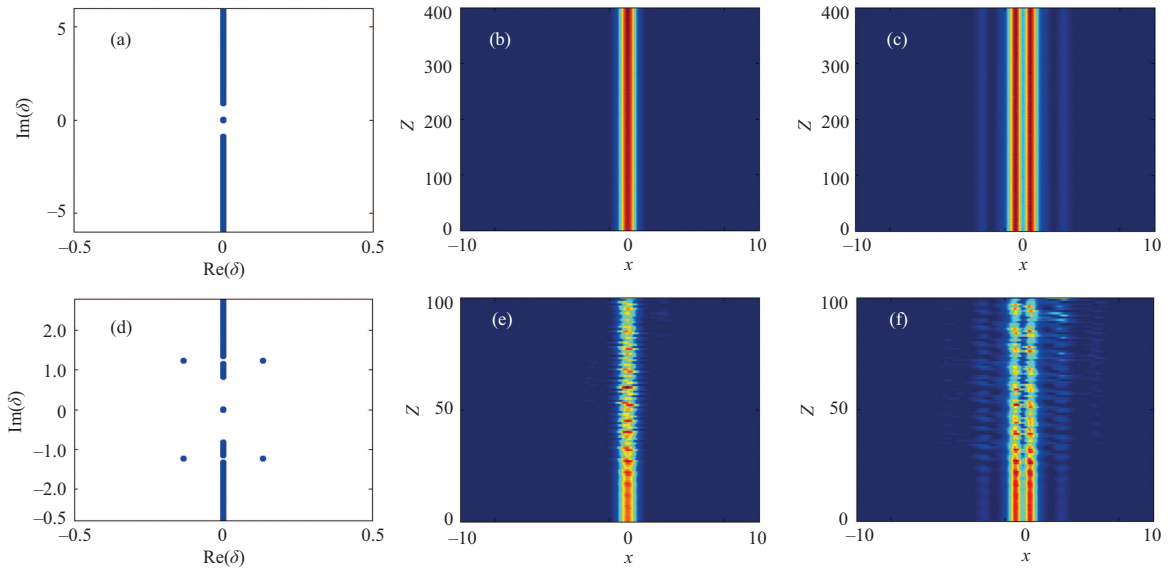


Fig. 3. (a) The linear-stability spectrum of the vector soliton for $\mu_2 = 1.5$. (b)–(c) The corresponding stable propagations of the two components. (d) The linear-stability spectrum of the vector soliton for $\mu_2 = 2$. (e)–(f) The corresponding unstable propagations of the two components. Here $\alpha = 1.8$, $W_{10} = 0.2$, $W_{20} = 0.5$, and $\mu_1 = 4.5$ in all panels.

In Figs. 2 and 3, we have discussed the properties of mixed-gap vector solitons as functions of μ_2 (the propagation constant

of the second component), for a large Lévy index. One may wonder how these properties change for different values of μ_1 (the propagation constant of the first component), also at a large Lévy index. This discussion is summarized in Figs. 4 and 5.

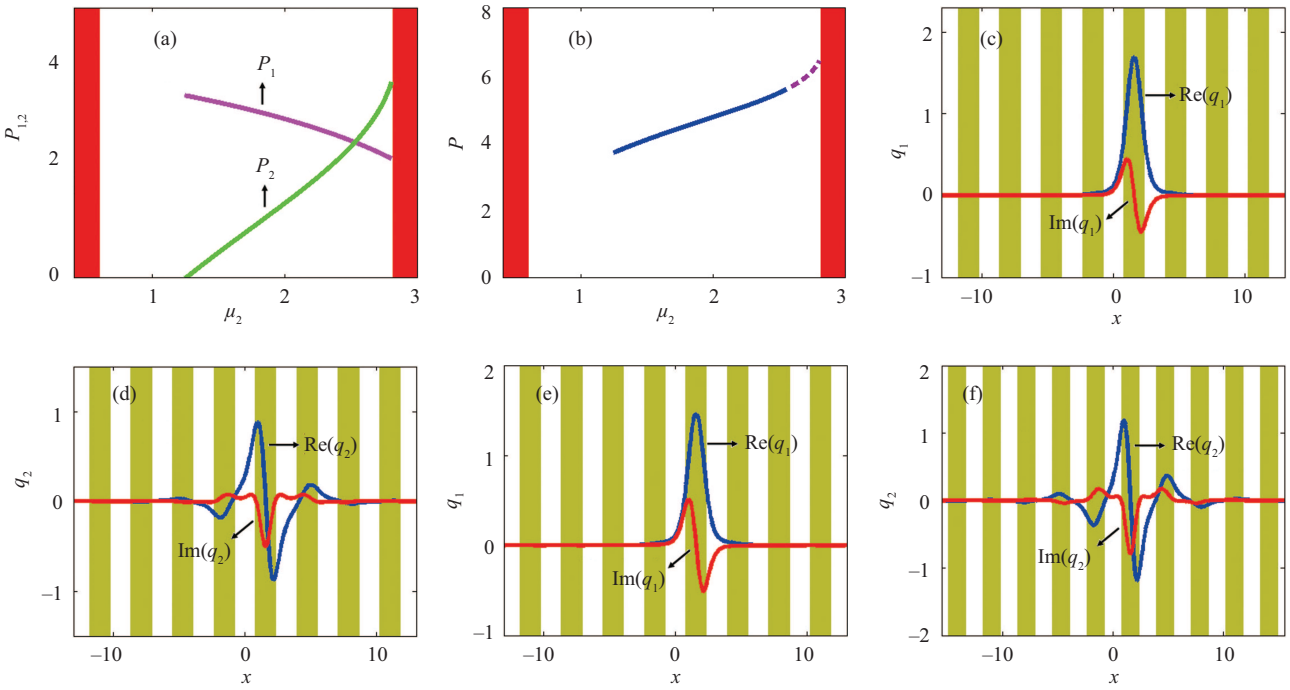


Fig. 4. Same as Fig. 2 but for $\mu_1 = 5.5$. Panels (c) and (d) are the profiles of the two components at $\mu_2 = 2$. Panels (e) and (f) are the profiles of the two components at $\mu_2 = 2.6$.

Based on our further study, we find that the propagation constant of the soliton's first component (μ_1) significantly influences the existence and stability of solitons. Recall that the value of μ_1 in Figs. 2 and 3 is fixed at $\mu_1 = 4.5$. Now, we investigate mixed-gap vector solitons for another value of μ_1, by setting $\mu_1 = 5.5$ in Figs. 4 and 5. The existence region for the soliton at $\mu_1 = 5.5$ is $1.26 \leq \mu_2 \leq 2.82$ (see also Figs. 4(a) and 4(b)). Remarkably, this soliton family can reach the lower edge of the first Bloch band. It should also be mentioned that solitons are stable in the low-power region of $1.26 \leq \mu_2 \leq 2.56$. According to Fig. 4(a), the soliton power of the first component decreases with μ_2, while the power of the second component increases with μ_2. Comparing the curves of Figs. 4(b) ($\mu_1 = 5.5$) and 2(b) ($\mu_1 = 4.5$) reveals that the stability domain for $\mu_1 = 5.5$ is wider than in Fig. 2(b). The profiles of solitons at $\mu_2 = 2$ and $\mu_2 = 2.6$ are presented in Figs. 4(c)–4(d) and 4(e)–4(f), respectively.

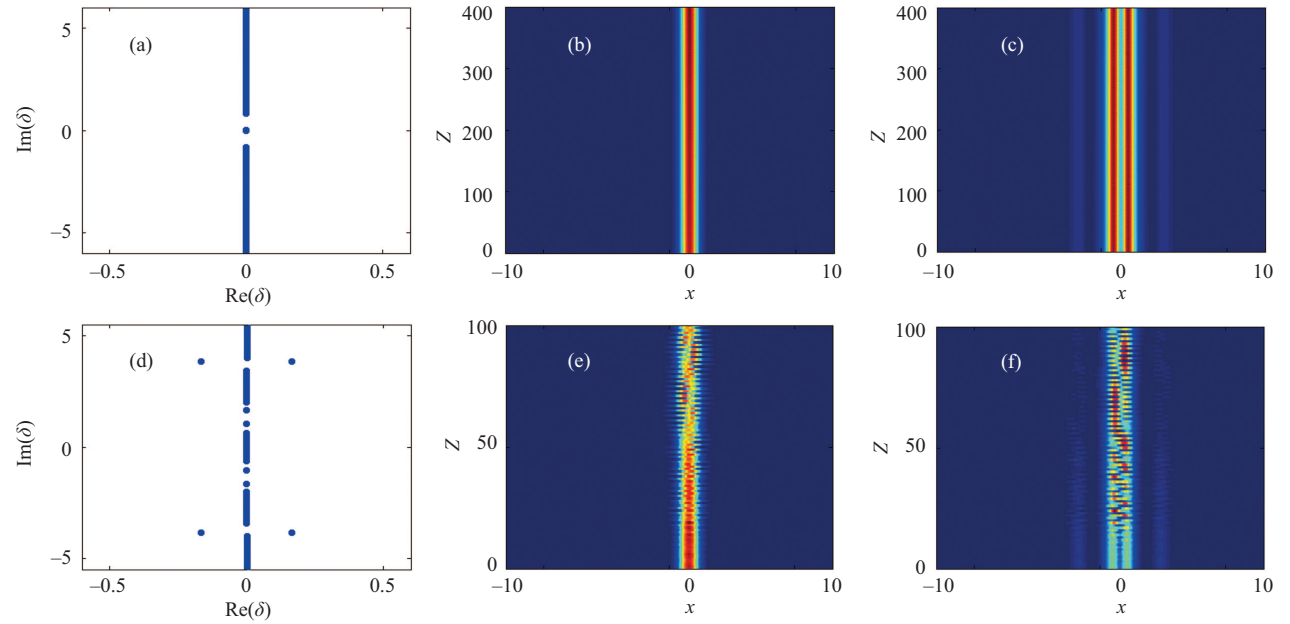


Fig. 5. Same as Fig. 3 but for $\mu_1 = 5.5$. Panels (a)–(c) are the linear-stability spectrum and propagations of two components at $\mu_2 = 2$. Panels (d)–(f) are the linear-stability spectrum and propagations of the two components at $\mu_2 = 2.6$.

Linear-stability spectra and perturbed propagations of typical examples of vector solitons from Fig. 2 are reported in Fig. 5. In particular, we present the spectrum and propagation of the soliton at $\mu_2 = 2$ [Figs. 4(c)–4(d)] in Figs. 5(a)–5(c). Similar to Fig. 3, the left column of Fig. 5 displays the spectrum [from Eqs. (9)], while the middle and right columns show the propagation of the first (U_1) and second (U_2) components, respectively. According to Fig. 5(a), the mixed-gap soliton at $\mu_2 = 2$ is stable. The corresponding propagation in Figs. 5(b) and 5(c) is consistent with the spectrum in Fig. 5(a). In addition, we display the spectrum and propagation of an unstable soliton at $\mu_2 = 2.6$, in Figs. 5(d)–5(f) [the corresponding profiles are reported in Figs. 4(e) and 4(f)]. It is seen in Fig. 5(d) that the real parts of two eigenvalues δ are greater than zero; thus this soliton is unstable. This can also be verified from propagations in Figs. 5(e) and 5(f), where both components undergo unacceptable distortions.

3.2. Vector solitons with a small Lévy index

In this subsection, we focus on the results for vector solitons with a small Lévy index; in particular, we set $\alpha = 1.3$. For this case, our model also supports mixed-gap vector solitons composed of a fundamental (the first component) and a dipole (the second component) mode, where the propagation constants belong to the semi-infinite and first band gaps, respectively. We present partial powers ($P_{1,2}$) and the total power (P) versus μ_2, for $W_{10} = 0.2$, $W_{20} = 0.5$, $\mu_1 = 5.5$, in Figs. 6(a) and 6(b). The solid and dashed lines in Fig. 6(b) represent the stable and unstable solutions, respectively. According to the results from Fig. 6(b), the existence and stability domains for this family of solitons are $1.58 \leq \mu_2 \leq 2.94$ and $1.58 \leq \mu_2 \leq 1.94$. In this case, the family can reach the lower edge of the first Bloch band, similar to the case with $\alpha = 1.8$, shown in Fig. 4(b). It should also be mentioned that such solitons are stable in a low-power region and unstable at higher powers, and the width of the stability domain is much smaller than that of $\alpha = 1.8$.

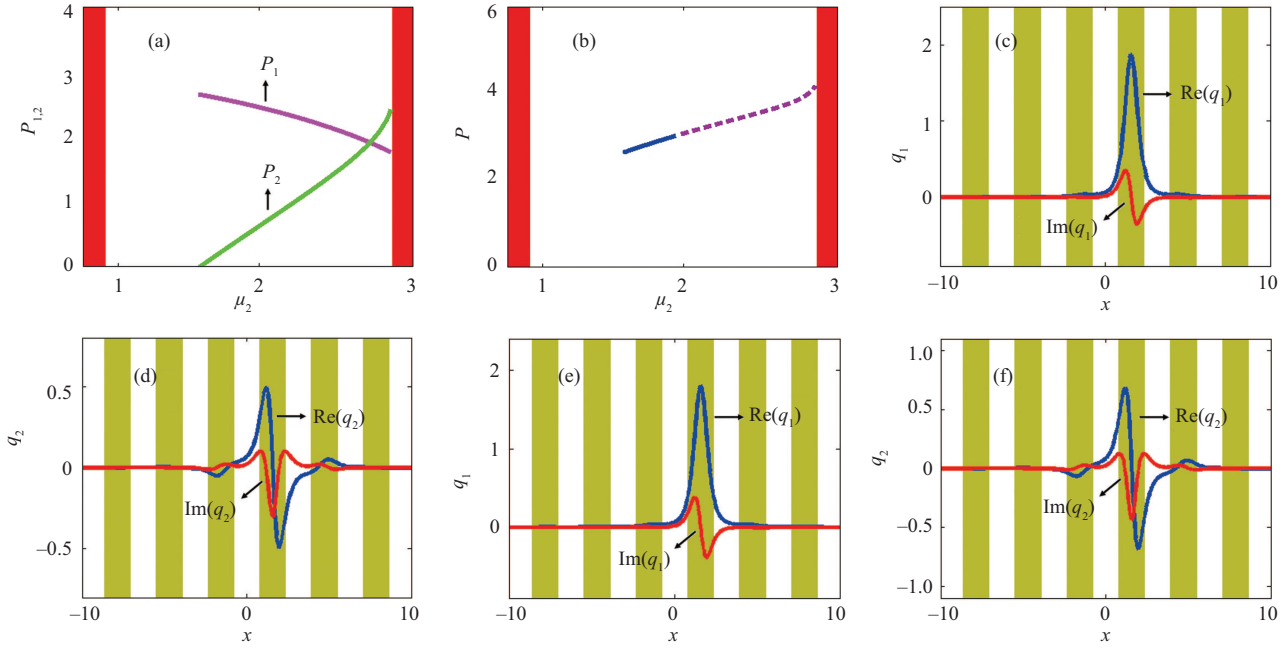


Fig. 6. (a) Partial powers of the two components of vector solitons (shades red regions are Bloch bands) *versus* the propagation constant μ_2. (b) The total power of vector solitons (solid and dashed lines represent stable and unstable solitons) *versus* μ_2. (c)–(d) The profiles of the first and second components of the vector soliton at $\mu_2 = 1.8$. (e)–(f) The profiles of the first and second components of the vector soliton at $\mu_2 = 2$. Here, $\alpha = 1.3$, $W_{10} = 0.2$, $W_{20} = 0.5$, and $\mu_1 = 5.5$ in all panels.

The profiles of the first and second components of the vector soliton at $\mu_2 = 1.8$ (in the first band gap) are portrayed in Figs. 6(c) and 6(d). We also report the profiles of the soliton at $\mu_2 = 2$ (also in the first finite gap), in Figs. 6(e) and 6(f). From panels (c)–(f), it is clear that the width of both components remains almost constant as μ_2 changes. Additionally, the amplitude of the first component (q_1) decreases with μ_2, while the amplitude of the second component (q_2) increases with μ_2, similar to previous results. This behavior is also evident from the curves of soliton powers P_1 and P_2 *versus* μ_2 in Fig. 6(a).

Linear-stability spectra and perturbed propagations of the mixed-gap vector soliton examples from Fig. 6 are reported in Fig. 7. In particular, the spectrum and propagation of the soliton at $\mu_2 = 1.8$ [from Figs. 6(c) and 6(d)] are shown in Figs. 7(a)–7(c). As before, the left column displays the spectrum, and the middle and right columns display the perturbed propagation of the first (U_1) and second (U_2) components, respectively. As seen in Fig. 7(a), the soliton at $\mu_2 = 1.8$ is stable

(all real parts of δ are equal to zero), which is also confirmed from its perturbed propagations, shown in Figs. 7(b) and 7(c). In contrast, the spectrum and propagation of an unstable soliton at $\mu_2 = 2$ are displayed in Figs. 7(d)–7(f) [the corresponding profiles are shown in Figs. 6(e) and 6(f)]. From Fig. 7(d), it is clear that the real parts of two eigenvalues δ are greater than zero; thus, this soliton is unstable. The instability is evident in perturbed propagations as shown in Figs. 7(e) and 7(f), where both the first and the second components suffer significant distortions.

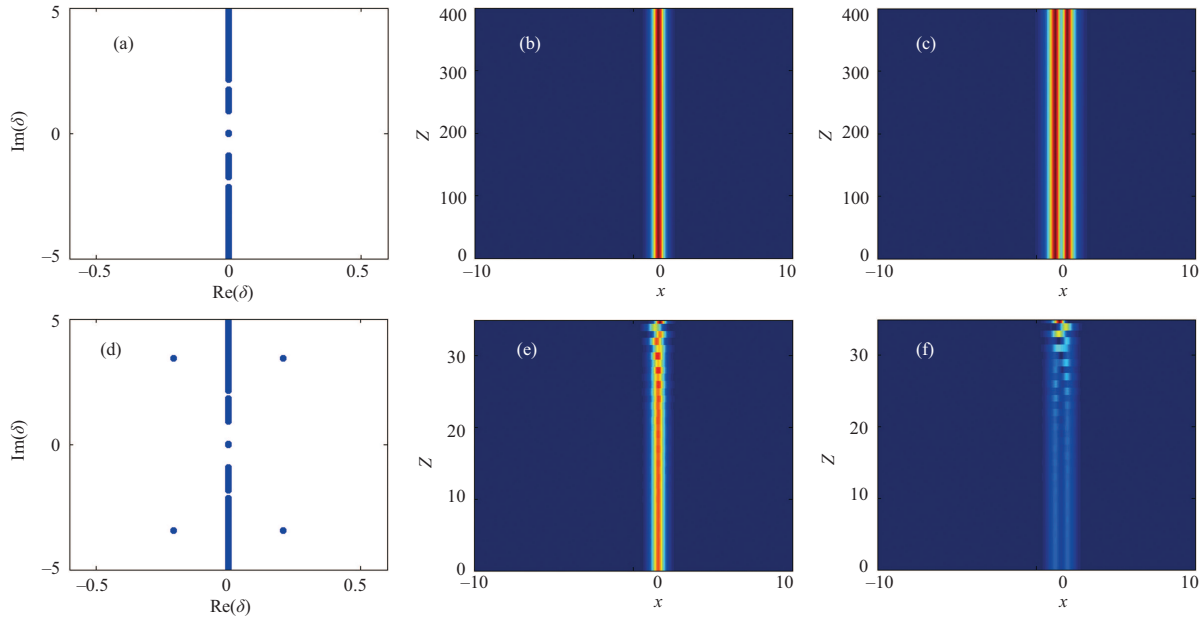


Fig. 7. (a) The linear-stability spectrum of the vector soliton at $\mu_2 = 1.8$. (b)–(c) The corresponding stable propagations of the two components. (d) The linear-stability spectrum of the vector soliton when $\mu_2 = 2$. (e)–(f) The corresponding unstable propagations of the two components. Here, $\alpha = 1.3$, $W_{10} = 0.2$, $W_{20} = 0.5$, and $\mu_1 = 5.5$ in all panels.

In Figs. 6 and 7, we discussed the properties of mixed-gap vector solitons for different values of μ_2, with a small Lévy index. We are curious how these solitons will change for different values of W_{20} (still at a small value of α). We focus on these topics in the next subsection and present the results in Figs. 8 and 9.

3.3. Vector solitons with a changing nonlinear potential

Based on our further study, we find that parameter W_{20} significantly influences the existence and stability of mixed-gap vector solitons in our model. Recall that the value of W_{20} was thus far fixed at $W_{20} = 0.5$. In Figs. 8 and 9, we investigate solitons for a different value, $W_{20} = 0.75$. For this value, the existence region of solitons is $1.65 \leq \mu_2 \leq 2.94$ (see Figs. 8(a) and 8(b)). Note that these solitons are stable only in the low-power part of this region, specifically for $(1.65 \leq \mu_2 \leq 1.73)$. As shown in Fig. 8(a), the soliton power of the first component decreases with increasing μ_2, while the power of the second component increases. A comparison of the curves in Figs. 8(b) ($W_{20} = 0.75$) and 6(b) ($W_{20} = 0.5$) reveals that the stability domain for $W_{20} = 0.75$ is much narrower, signifying that the critical value is being approached. In fact, for $W_{20} \geq 0.89$, all solitons become unstable, indicating that the threshold value apparently is $W_{20}^{\text{th}} = 0.89$. We portray the profiles of solitons at $\mu_2 = 1.7$ and $\mu_2 = 1.8$ in Figs. 8(c), 8(d), 8(e), and 8(f), respectively.

For completeness, we also report on the stability of mixed-gap vector solitons as W_{10} increases. We increase W_{10} to 0.25 while keeping W_{20} fixed at 0.5. Both large and small values of α are considered. For a large α (α=1.8) with $\mu_1 = 4.5$, the stability domain of these vector solitons is $1.00 \leq \mu_2 \leq 1.60$. When $\mu_1 = 5.5$, the corresponding stability range is $1.29 \leq \mu_2 \leq 2.34$. For a small α ($\alpha = 1.3$) with $\mu_1 = 5.5$, the stability domain is $1.52 \leq \mu_2 \leq 1.67$. Generally, the stability ranges of the solitons narrow as W_{10} increases, mirroring the behavior observed when W_{20} increases. However, for $\alpha = 1.3$, $\mu_1 = 5.5$, and $W_{20} = 0.75$, all such mixed-gap vector solitons are unstable. Furthermore, compared to the case of $W_{10} = 0.2$, all the stability domains mentioned above become smaller.

Finally, we display the linear-stability spectra and perturbed propagations for the soliton examples from Fig. 8 in Fig. 9. The spectrum and propagation of the soliton at $\mu_2 = 1.7$ in Figs. 8(c) and 8(d) are presented in Figs. 9(a)–9(c). As before, the left column of Fig. 9 portrays the spectrum, while the middle and right columns depict propagations of the first (U_1) and second (U_2) components. It is clear that the soliton shown in Figs. 9(a)–9(c) (at $\mu_2 = 1.7$) is stable. On the other hand, we present the spectrum and propagation of an unstable vector soliton at $\mu_2 = 1.8$ in Figs. 9(d)–9(f).

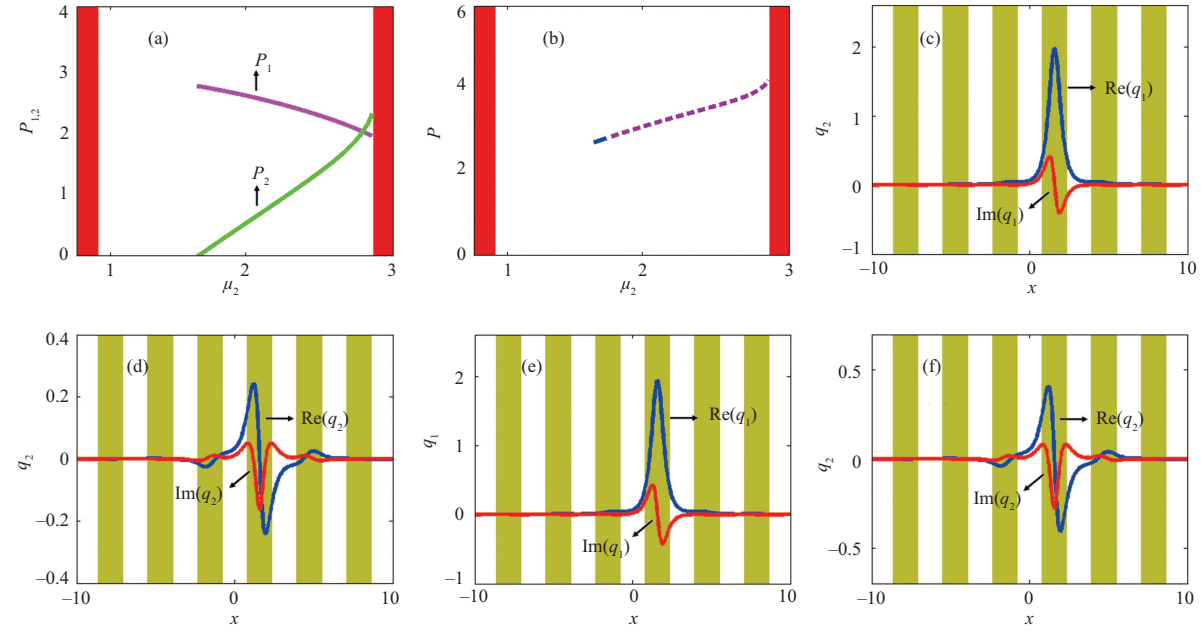


Fig. 8. Same as Fig. 6 but for $W_{20} = 0.75$. Panels (c) and (d) are the profiles of the two components at $\mu_2 = 1.7$. Panels (e) and (f) are the profiles of the two components at $\mu_2 = 1.8$.

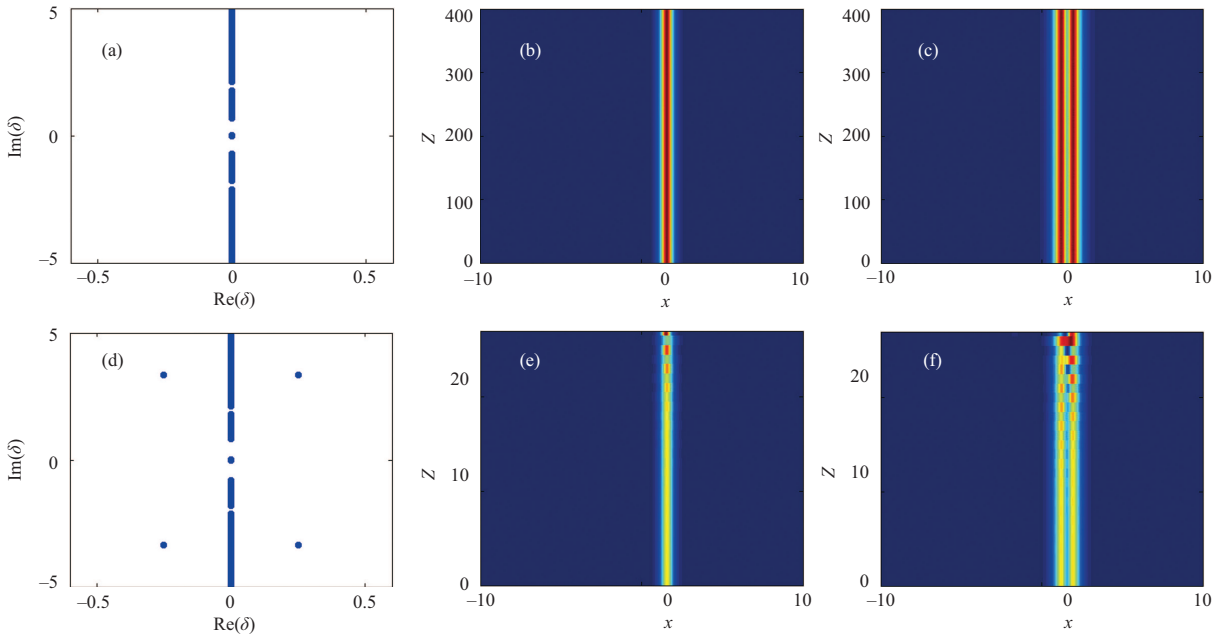


Fig. 9. Same as Fig. 7 but for $W_{20} = 0.75$. Panels (a)–(c) are the linear-stability spectrum and propagations of two components at $\mu_2 = 1.7$. Panels (d)–(f) are the linear-stability spectrum and propagations of the two components at $\mu_2 = 1.8$.

4. Conclusion

In conclusion, we have demonstrated that mixed-gap vector solitons can be supported by the coupled nonlinear Schrödinger equations in cubic nonlinear media with $\mathcal{PT}$-symmetric mixed linear–nonlinear lattices and fractional diffraction. We focused on vector solitons whose first component is a fundamental soliton and whose second component is a dipole soliton. When the propagation constant of the first component μ_1 is fixed, the soliton power of the first component P_1 decreases as the propagation constant μ_2 of the second component increases, whereas the power P_2 of the second component increases with μ_2. We investigated this behavior for both large and small values of the Lévy index. Notably, the stability domains of vector solitons with a large Lévy index are always much wider than those with a small Lévy index. These stability domains were determined by the method of linear stability analysis and confirmed by direct numerical simulations.

Acknowledgements

Project supported by the National Natural Science Foundation of China (Grant Nos. 62205224 and 11774068), the

Guangdong Basic and Applied Basic Research Foundation (Grant No. 2023A1515010865), the Guangzhou Science and Technology Plan Project (Grant No. 2025A04J4068), the Tertiary Education Scientific Research Project of Guangzhou Municipal Education Bureau (Grant No. 2024312022), and the Qatar National Research Fund (Grant No. NPRP13S-0121-200126).

References

[1] Kivshar Y S and Malomed B A 1989 *Rev. Mod. Phys.* **61** 763
[2] Kartashov Y V, Malomed B A and Torner L 2011 *Rev. Mod. Phys.* **83** 247
[3] Konotop V V, Yang J and Zezyulin D A 2016 *Rev. Mod. Phys.* **88** 035002
[4] Leblond L and Mihalache D 2013 *Phys. Rep.* **523** 61
[5] Kartashov Y V, Astrakharchik G E, Malomed B A and Torner L 2019 *Nat. Rev. Phys.* **1** 185
[6] Mihalache D, Mazilu D, Lederer F, Malomed B A, Kartashov Y V, Crasovan L C and Torner L 2005 *Phys. Rev. Lett.* **95** 023902
[7] Belić M, Petrović N, Zhong W P, Xie R H and Chen G 2008 *Phys. Rev. Lett.* **101** 123904
[8] Zhang P, Hu C, Zhou Q, Biswas A and Liu W 2020 *Nonlinear Dyn.* **101** 1215
[9] Zhu X, Peng X, Qiu Y, Wang H and He Y 2020 *New J. Phys.* **22** 033035
[10] Zhou Q, Zhong Y, Triki H, Sun Y, Xu S, Liu W and Biswas A 2022 *Chin. Phys. Lett.* **39** 044202
[11] Si Z Z, Wang D L, Zhu B W, Ju Z T, Wang X P, Liu W, Malomed B A, Wang Y Y and Dai C Q 2024 *Laser Photon. Rev.* **18** 2400097
[12] Zeng L, Belić M R, Mihalache D and Zhu X 2024 *Chaos, Solitons and Fractals* **181** 114645
[13] Frantzeskakis D J 2010 *J. Phys. A* **43** 213001
[14] Lobanov V E, Kartashov Y V and Konotop V V 2014 *Phys. Rev. Lett.* **112** 180403
[15] Bagnato V S, Frantzeskakis D J, Kevrekidis P G, Malomed B A and Mihalache D 2015 *Rom. Rep. Phys.* **67** 5
[16] Kartashov Y V and Zezyulin D A 2019 *Phys. Rev. Lett.* **122** 123201
[17] Kartashov Y V and Konotop V V 2020 *Phys. Rev. Lett.* **125** 054101
[18] Zhu X, Xiang D and Zeng L 2023 *Chaos, Solitons and Fractals* **169** 113317
[19] Mihalache D 2024 *Rom. Rep. Phys.* **76** 402
[20] Aceves A B 2000 *Chaos* **10** 584
[21] Kartashov Y V, Vysloukh V A and Torner L 2008 *Opt. Lett.* **33** 1774
[22] Ju Z T, Si Z Z, Yan X and Dai C Q 2024 *Chin. Phys. Lett.* **41** 084203
[23] Zhu X, Belić M R, Mihalache D, Xiang D and Zeng L 2025 *Opt. Laser Technol.* **184** 112426
[24] Zeng X, Belić M R, Mihalache D, Lu X, Cai Y, Li J, Zhu X and Zeng L 2025 *Opt. Express* **33** 33483
[25] Zeng L, Wang T, Belić M R, Mihalache D and Zhu X 2024 *Nonlinear Dyn.* **112** 22283
[26] Kartashov Y V, Ye F, Konotop V V and Torner L 2021 *Phys. Rev. Lett.* **127** 163902
[27] Zeng L, He J, Malomed B A, Chen J and Zhu X 2024 *Phys. Rev. E* **110** 064216
[28] Zeng L, Malomed B A, Mihalache D, Li J and Zhu X 2024 *Opt. Lett.* **49** 6944
[29] Kartashov Y V, Malomed B A, Vysloukh V A and Torner L 2009 *Opt. Lett.* **34** 770
[30] Zhu X, Fan Y, Belić M R, Mihalache D, Xiang D and Zeng L 2025 *Opt. Express* **33** 7205
[31] Shao K H, Li B L, Xi Z H, Tu P, Wang Q Q, Ma J P, Zhao X and Shi Y R 2024 *Chin. Phys. B* **33** 060501
[32] Zeng Y W, Yang T L, Lin Q Y and Su W J 2024 *Chin. Phys. B* **33** 124201
[33] Krasnok A, Nefedkin N and Alu A 2021 *IEEE Antennas and Propagation Magazine* **63** 110
[34] Bender C M and Boettcher S 1998 *Phys. Rev. Lett.* **80** 5243
[35] Bender C M, Boettcher S and Meisinger P N 1999 *J. Math. Phys.* **40** 2201
[36] Bender C M, Brody D C and Jones H F 2002 *Phys. Rev. Lett.* **89** 270401
[37] Suchkov S V, Sukhorukov A A, Huang J, Dmitriev S V, Lee C and Kivshar Y S 2016 *Laser Photon. Rev.* **10** 177
[38] Muniz A L, Wimmer M, Bisianov A, Peschel U, Morandotti R, Jung P S, Christodoulides D N 2019 *Phys. Rev. Lett.* **123** 253903
[39] Musslimani Z H, Makris K G, El-Ganainy R and Christodoulides D N 2008 *Phys. Rev. Lett.* **100** 030402
[40] Abdullaev F Kh, Kartashov Y V, Konotop V V and Zezyulin D A 2011 *Phys. Rev. A* **83** 041805
[41] Driben R and Malomed B A 2011 *Opt. Lett.* **36** 4323
[42] Zhu X, Wang H, Zheng L X, Li H and He Y J 2011 *Opt. Lett.* **36** 2680
[43] Zezyulin D A and Konotop V V 2012 *Phys. Rev. Lett.* **108** 213906
[44] Jisha C P, Jisha A, Brazhnyi V A and Assanto G 2014 *Phys. Rev. A* **89** 013812
[45] Liu X M, Zhang Z Y and Liu W J 2023 *Chin. Phys. Lett.* **40** 070501
[46] Li BB, Zhao Y, Xu S L, Zhou Q, Fu Q D, Ye F W, Hua C B, Chen M W, Hu H J, Zhou Q Q and Qiu Z C 2023 *Chin. Phys. Lett.* **40** 044201
[47] Wang L, Zeng J and Zhu Y 2024 *Physica D* **465** 134144
[48] Fan Z, Shi Y, Wang H, Zhao Y, Peng W and Xu S 2024 *Chin. Phys. B* **33** 120306
[49] Wimmer M, Regensburger A, Miri M A, Bersch C, Christodoulides D N and Peschel U 2015 *Nat. Commun.* **6** 7782
[50] Laskin N 2000 *Phys. Lett. A* **268** 298
[51] Laskin N 2000 *Phys. Rev. E* **62** 3135
[52] Laskin N 2002 *Phys. Rev. E* **66** 056108
[53] Stickler B A 2013 *Phys. Rev. E* **88** 012120
[54] Longhi S 2015 *Opt. Lett.* **40** 1117
[55] Malomed B A 2021 *Photonics* **8** 353
[56] Malomed B A 2024 *Chaos* **34** 022102
[57] Huang C, Deng H, Zhang W, Ye F and Dong L 2018 *Europhys. Lett.* **122** 24002
[58] Huang C and Dong L 2016 *Opt. Lett.* **41** 5636
[59] Su W, Deng H, Dong L, Huang Z and Huang C 2020 *Chaos, Solitons and Fractals* **141** 110427
[60] Zeng L and Zeng J 2019 *Opt. Lett.* **44** 2661
[61] Gao X, Belić M R, Mihalache D, Shi J, Zhu X and Zeng L 2025 *Phys. Lett. A* **563** 131042
[62] Li P, Malomed B A and Mihalache D 2020 *Opt. Express* **28** 34472
[63] Zhong W P, Belić M R, Malomed B A, Zhang Y and Huang T 2016 *Phys. Rev. E* **94** 012216
[64] Mejía-Cortés C and Molina M I 2021 *Opt. Lett.* **46** 2256
[65] Zhong M, Chen Y, Yan Z and Malomed B A 2024 *Physica D* **462** 134157
[66] Huang C and Dong L 2019 *Opt. Lett.* **44** 5438
[67] Zeng L, Belić M R, Mihalache D, Li J, Xiang D, Zeng X and Zhu X 2023 *Physica D* **456** 133924
[68] Mihalache D, Mazilu D and Torner L 1998 *Phys. Rev. Lett.* **81** 4353
[69] Krolikowski W, Ostrovskaya E A, Weilnau C, Geisser M, McCarthy G, Kivshar Y S, Denz C and Luther-Davies B 2000 *Phys. Rev. Lett.* **85** 1424
[70] Yang J and Tan Y 2000 *Phys. Rev. Lett.* **85** 3624
[71] Kartashov Y V 2013 *Opt. Lett.* **38** 2600
[72] Yang J and Lakoba T I 2007 *Stud. Appl. Math.* **118** 153
[73] Yang J 2010 *Nonlinear Waves in Integrable and Nonintegrable Systems* (SIAM)